Alternative S2 Hinge Regions of the Myosin Rod Affect Myofibrillar Structure and Myosin Kinetics

Mark S. Miller,[†*] Corey M. Dambacher,[‡] Aileen F. Knowles,[§] Joan M. Braddock,[†] Gerrie P. Farman,[¶] Thomas C. Irving,[¶] Douglas M. Swank,[‖] Sanford I. Bernstein,[‡] and David W. Maughan[†]

[†]Department of Molecular Physiology and Biophysics, University of Vermont, Burlington, Vermont; [‡]Department of Biology, Molecular Biology Institute and SDSU Heart Institute, [§]Department of Chemistry and Biochemistry, San Diego State University, San Diego, California; [¶]Biophysics Collaborative Access Team and Center for Synchrotron Radiation Research and Instrumentation, Department of Biological, Chemical, and Physical Sciences, Illinois Institute of Technology, Chicago, Illinois; and [‖]Department of Biology and Center for Biotechnology and Interdisciplinary Studies, Rensselaer Polytechnic Institute, Troy, New York

ABSTRACT The subfragment 2/light meromyosin "hinge" region has been proposed to significantly contribute to muscle contraction force and/or speed. Transgenic replacement of the endogenous fast muscle isovariant hinge A (exon 15a) in *Drosophila melanogaster* indirect flight muscle with the slow muscle hinge B (exon 15b) allows examination of the structural and functional changes when only this region of the myosin molecule is different. Hinge B was previously shown to increase myosin rod length, increase A-band and sarcomere length, and decrease flight performance compared to hinge A. We applied additional measures to these transgenic lines to further evaluate the consequences of modifying this hinge region. Structurally, the longer A-band and sarcomere lengths found in the hinge B myofibrils appear to be due to the longitudinal addition of myosin heads. Functionally, hinge B, although a significant distance from the myosin catalytic domain, alters myosin kinetics in a manner consistent with this region increasing myosin rod length. These structural and functional changes combine to decrease whole fly wing-beat frequency and flight performance. Our results indicate that this hinge region plays an important role in determining myosin kinetics and in regulating thick and thin filament lengths as well as sarcomere length.

INTRODUCTION

The full-length myosin II molecule can be divided into three regions using proteolysis: the subfragment 1 or S1 (N-terminal globular head), subfragment 2 or S2 (intermediate region between the myosin head and rod), and light meromyosin or LMM (C-terminal portion of the myosin rod). Connecting these three regions are two ''hinges'' that may prove functionally important to the performance of myosin. The S1/S2 hinge joins the S1 and S2 regions and may serve to orient the myosin head toward the thin filament. The S2/LMM hinge, which is the subject of this study, joins the S2 and LMM regions and is an ~152 amino acid section that can be cleaved from the C-terminus of the S2 region with prolonged digestion by trypsin (1,2) (cf. Fig. 1 of Suggs et al. (3)). The S2/LMM hinge region may allow the myosin head to move away from the thick filament and closer to the thin filament (4,5) since most of the S2 region is loosely attached to the thick filament (6,7). The central area of the S2/LMM hinge may be flexible but does not appear to kink; instead, kinking of the myosin rod occurs at 44 and 76 nm from the end of the globular head near the boundaries of the S2/LMM hinge (8). A unique predicted property of the S2/LMM hinge region is a reduced propensity to form an α-helical coiled-coil (9); instead, portions form shorter random coils that potentially have increased longitudinal (10) and torsional (11) flexibility. A coiled-coil to random coil transition, or melting, that causes the S2/LMM hinge region to shorten can be induced by increasing temperature or pH (5,12,13).

The importance of the S2/LMM hinge region has been suggested by correlating the type of hinge incorporated into the myosin heavy chain (MHC) and the muscle's mechanical performance in invertebrates (scallop: fast striated versus slow catch smooth MHC (14); *Drosophila melanogaster*: fast versus slow contracting MHC (15,16)) and vertebrates (rat: α- versus β-MHC (17); human: six skeletal muscle MHCs (18)). These examples suggest that the S2/LMM hinge has a significant role in muscle contraction; however, the alternative isoforms harbor additional differences in other regions of their MHCs that may influence performance. Nevertheless, evidence for the importance of the S2/LMM hinge has been obtained by examining the effect of binding antibodies to this region. In skeletal muscle myofibrils, hinge region antibodies decreased active isometric tension and myofibril stiffness without changing maximum shortening velocity or Mg^{2+}-ATPase (19–21). In cardiac myocytes, an antibody decreased maximum shortening velocity without affecting ATPase (22). Although these studies indicate that the hinge region is important to contraction, the precise role of the S2/LMM hinge region remains unclear.

The known genetics of the S2/LMM hinge region in *D. melanogaster*, the relative ease of producing mutations in this species, the ability to measure the mechanical properties of indirect flight muscle (IFM) fibers (23), and the availability

Submitted September 10, 2008, and accepted for publication January 8, 2009.

*Correspondence: Mark.Miller@uvm.edu

C. M. Dambacher's present address is Scripps Research Institute, Department of Chemistry and Skaggs Institute for Chemical Biology, La Jolla, California.

Editor: Shin'ichi Ishiwata.

0006-3495/09/05/4132/12 $2.00

doi: 10.1016/j.bpj.2009.02.034

of adequate myosin from this tissue for steady-state kinetics and in vitro motility assays (24) provide investigators a unique opportunity to structurally and functionally compare *Drosophila* myosin molecules that differ only in their S2/LMM hinge region. *Drosophila* has a single gene encoding MHC, and isoforms of the protein result from alternative splicing of the primary RNA transcript (25). The central 26 amino acids of the S2/LMM hinge region are encoded by the alternative exons 15a and 15b, and all the other regions along the coiled-coil are invariant (15,25). The central amino acid sequence encoded by exon 15a (hinge A: AEHDRQTC HNELNQTRTACDQLGRDK) has a net charge of +1 and 4 hydrophobic residues, whereas the exon 15b-encoded sequence (hinge B: AEKEKNEYYGQLNDLRAGVDHIT NEK), which has only seven amino acids in common with hinge A, has a net charge of −1 and 8 hydrophobic residues (3). Hinge A is expressed in muscles that contract frequently and quickly (IFM) or have a high active tension (jump muscles). Hinge B is expressed in muscles that contract slowly (larval and adult body wall), whereas intermediate speed muscles (leg and proboscis) contain myosins with hinge A and myosins with hinge B (15,16). These results suggest that the two alternative S2/LMM hinges contribute to differences in functional performance between muscle types.

In a previous study that examined functional differences between the alternative S2/LMM hinges, hinge A in the IFM and jump muscles (tergal depressor of the trochanter or TDT) was transgenically replaced by hinge B (3). These hinge-switch mutants, which express hinge B in their IFM and TDT, had severely compromised flight and jump ability, clearly showing that the hinge region is important for whole-muscle performance. A detailed structural analysis of the IFM muscles revealed that the hinge-switch lines had increased sarcomere length, thick filament length, and MHC rod length compared to transgenic controls, indicating that the hinge region plays an important role in the assembly of the myofilament lattice. In the study presented here, we sought to determine the reason for the increased A-band length and decreased IFM performance in flies expressing hinge B. Our structural results indicate that the increased A-band length is due to an increased number of longitudinally incorporated myosin molecules making the thick filaments longer. A detailed mechanical evaluation of hinge-switch and control IFM fibers revealed changes in myosin kinetics, which are consistent with the S2/LMM hinge region increasing the length of the myosin rod. Overall, we conclude that the decreases in whole-fly performance after the replacement of hinge A with hinge B are driven by the increase in sarcomere length and alterations in myosin kinetics.

MATERIALS AND METHODS

Fly stocks and transgenic construction

Construction of the transgenes and preparation of transgenic lines by *P*-element-mediated transformation were performed as previously described (3,26). Briefly, all *Drosophila* lines used in this study contain a mutation in the genomic *Mhc* gene that eliminates expression of the endogenous MHC isoform in the IFM (15). Both the *15b-47* and *15b-108* adult fly lines express the same embryonic version of MHC with the S2 hinge B, but differ in transgene insertion point (3). The *15b-47* and *15b-108* lines were selected for these experiments because their general ultrastructures closely resemble those of the wild-type, in contrast to another independently generated line, *15b-3*, in which flies occasionally have severe ultrastructural defects (3). The control for the whole-fly and single muscle-fiber experiments was the *PwMhc2* line, which expresses all wild-type MHC isoforms from a transgenic source (26).

Flight performance

Flight tests involved releasing individual 2- to 3-day-old female flies from the center of a plexiglas flight chamber with a light source at the top (27) and scoring their flight as up (U), horizontal (H), down (D), or not at all (N). The flight index was determined using the formula 6*U/T + 4*H/T + 2*D/T + 0*N/T, where U, H, D, and N are the number of flights in each category of flight ability, and T is the total number of flies tested (28). Wing-beat frequency was measured on 2- to 3-day-old tethered female flies by means of an optical tachometer as previously described (29). Flight performance was measured at room temperature (22°C) and the temperature at which single-fiber muscle mechanics were performed (15°C).

Electron microscopy

Length estimates of the A-band bare zone and actin filaments were performed on images that had been prepared for and described in a previous study comparing the hinge-switch lines with the transgenic control (3).

X-ray diffraction

Live flies were prepared for the x-ray beam as described previously (30). Resting (wings folded) live fly muscle x-ray diffraction patterns were obtained using the small angle instrument on the Biophysics Collaborative Access Team (BioCAT) beam line (31) at the Advanced Photon Source (Argonne, IL) and analyzed as previously described (30). The peak intensity, widths, and peak separations for the 1,0 and 2,0 equatorial reflections were estimated using a nonlinear least-squares fitting procedure as described previously (32). The ratio of the 2,0 and 1,0 equatorial reflections, $I_{2,0}/I_{1,0}$, is a measure of the shift of cross-bridge mass between the thick and thin filaments (33). The separation of the 1,0 equatorial reflections was transformed into the distance between the lattice planes of the thick filaments ($d_{1,0}$), which was converted to interfilament spacing ($d_{1,0} \times 2/\sqrt{3}$), giving the center-to-center distance between thick filaments (34). The 14.5 nm spacing of the near meridional reflection is a measure of the distance between the center of mass of the cross-bridges (33). The 14.5 intensity indicates the cross-bridge angle in relation to the long axis of the thick filament; it is weakest when the cross-bridges are at oblique angles or distributed over a wide range of axial angles, and increases as the population of cross-bridges perpendicular to the filament axis increases (33). The disorder parameter (σ_s) is related to the amount of paracrystalline "liquid-like" disorder of the myofilaments in the hexagonal lattice (35).

Single muscle-fiber solutions

Solutions were prepared according to a computer program that solves the ionic equilibria (36). Concentrations are expressed in mmol/L (mM) unless otherwise indicated. The relaxing solution consisted of pCa 8, 20 *N,N*-bis[2-hydroxyethyl]-2-aminoethanesulfonic acid (BES), 15 creatine phosphate (CP), 240 U/mL creatine phosphokinase (CPK), 1 DTT, 5 EGTA, 1 Mg^{2+}, 5 MgATP, 8 P_i, ionic strength of 200 mEq adjusted with sodium methane sulfate, and pH 7.0. The activating solution was the same as the relaxing solution except that it contained pCa 4.0. The rigor solution was

the same as the activating solution except that it lacked CP, CPK, and MgATP. The storage solution consisted of pCa 8, 20 BES, 10 DTT, 5 EGTA, 1 Mg^{2+}, 5 MgATP, 0.25 P_i, a protease inhibitor cocktail (Roche), ionic strength of 175 mEq adjusted with sodium methane sulfate, pH 7.0, with 50% w/v glycerol subsequently added. The skinning solution was the same as the storage solution except that it contained 0.5% Triton X-100.

Single muscle-fiber mechanics

Single dorsolongitudinal IFM fibers, isolated from split thoraces of 2- to 3-day-old female *D. melanogaster*, were cut in half lengthwise (to ~100 μm diameter) to reduce the cross-sectional area (CSA) and thus facilitate quicker diffusion of solutions. The fibers were demembranated in skinning solution for 1 h at 4°C, clipped with aluminum T-clips at both ends ~300 μm apart, and either immediately used for mechanical experiments or transferred to storage solution at −20°C and used within a few days of dissection. Fibers were mounted between a piezoelectric motor (Physik Instrumente, Auburn, MA) and a strain gauge (SensorNor, Horten, Norway) (37), and lowered into 30 μL of relaxing solution maintained at 15°C. The fiber was stretched from just taut to 5% over its just taut length in 1% increments. Fibers were activated (pCa 5.0) by three exchanges of equal amounts of bathing solution with activating solution and then stretched by 2% increments until oscillatory work production, evaluated by sinusoidal analysis, was maximized. Subsequently, the fibers were returned to relaxing solution (pCa 8.0) and progressively calcium-activated (from pCa 8.0 to pCa 4.5) with isometric tension measured and sinusoidal analysis performed at each calcium level. Individual recordings of normalized isometric tension were fit to the Hill equation $[Ca^{2+}]^n/([Ca^{2+}]_{50}{}^n + [Ca^{2+}]^n)$, where $[Ca^{2+}]_{50}$ = calcium concentration at half activation, $pCa_{50} = -\log [Ca^{2+}]_{50}$, and n = Hill coefficient. At the end of the experiment, the isometric tension and sinusoidal analysis measurements were recorded in rigor solution.

To perform sinusoidal analysis, we applied small-amplitude sinusoidal length changes (0.125% muscle length) to the fiber at 47 frequencies (0.5–1000 Hz) while measuring the force response (37). Length and force were normalized to determine strain ($\Delta L/L$) and tension (F/CSA) by dividing the length change (ΔL) by total fiber length (L), and by dividing the force (F) by the fiber cross-sectional area (CSA). An elliptical CSA was assumed and determined by measuring the top and side fiber diameter. Elastic (E_e) and viscous (E_v) moduli were calculated from the tension transient by determining the magnitudes of the in-phase and out-of-phase components (0° and 90° with respect to strain, respectively) (38). The elastic and viscous moduli are the real and imaginary parts, respectively, of the complex modulus, the ratio of the tension response to the strain. Work (J m^{-3}) and Power (W m^{-3}) generated by the muscle fiber were calculated from Work $= \pi\, f\, t\, (-E_v)\, (L_{amp})^2$ and Power $= \pi\, f\, (-E_v)\, (L_{amp})^2$, where f is the frequency of the length perturbations (Hz), t is the time needed to perform the length perturbations (s), E_v is the viscous modulus (kN/m^2), and the fractional change in length (L_{amp}) is 0.00125. Note that positive power output results from a negative viscous modulus.

Myosin and actin isolation

Myosin for the in vitro motility and ATPase assays was isolated from dorsolongitudinal IFMs of 120–200 flies as described previously (39). Wild-type myosin was isolated from either wild-type (*yw*) or *PwMhc2* fly lines, and *15b* myosin was from *15b-47* or *15b-108*. Acetone powder was made from chicken pectoralis muscle and used for extraction of G-actin according to methods described previously (40). Small aliquots of G-actin were stored in buffer containing 2 mM TrisCl, pH 8, 0.2 mM ATP, 0.2 mM $CaCl_2$, and 1 mM DTT at −80°C. For the preparation of F-actin, the G-actin solution was thawed and diluted to 33 μM with the buffer described above. One volume of 10× polymerization buffer (50 mM TrisCl, pH 8.0, 0.5 M KCl, 20 mM $MgCl_2$, and 10 mM ATP) was added to 9 volumes of the G-actin. Polymerization was allowed to proceed for a minimum of 4 h before use. The F-actin was stored at 4°C and used within 1–2 months.

ATPase determination

Actin-stimulated ATPase activity was determined in a reaction mixture (150 μL) consisting of 10 mM imidazole, pH 6.0, 20 mM KCl, 1 mM $MgCl_2$, 0.1 mM $CaCl_2$ 1 mM [γ-^{32}P]ATP, 0-2 μM F-actin, and ~2 μg of myosin. Myosin (1 μL of 2 μg/μL) was added to 134 μL of reaction mixture containing F-actin and allowed to incubate for 10 min at 23°C. The reaction was started by the addition of 15 μL of 10 mM [γ-^{32}P]ATP (~1000–1500 cpm/nmole ATP). After 30 min at 23°C, the reaction was terminated by the addition of 50 μL of 1.8 N $HClO_4$. An aliquot (0.1 mL) of the reaction mixture was used for extraction of ^{32}Pi for Cerenkov counting as described previously (41).

In vitro motility assay

In vitro actin sliding velocity assays were performed as previously described (42). Analysis of captured video sequences was performed as previously described (43), using modifications previously detailed (41).

Statistical analysis

All values are mean ± SE. Statistical analyses were performed using SPSS (v.14.0; SPSS, Chicago, IL). Statistical tests were considered significant at the $p < 0.05$ level, unless otherwise noted. For data comparing two myosin types (ATPase and in vitro motility), t-tests were performed. For most of the data comparing three strains (flight performance, x-ray diffraction, and single-fiber muscle mechanics), a one-way analysis of variance (ANOVA) was performed. If differences were significant, the Student-Neuman-Keuls (SNK) post-hoc test was used to determine which means differed. The only exceptions were variables, such as elastic or viscous moduli, that were examined across different sinusoidal oscillation frequencies. In this case, a repeated-measures ANOVA with frequency as the repeated measure was performed first. If a significant strain-specific effect was found between subjects, then one-way ANOVAs were performed at each frequency to determine significant differences.

RESULTS

Flight performance

Flight index and wing-beat frequency were dramatically decreased in both hinge-switch lines compared to the transgenic control at room temperature (22°C) and the temperature at which single-fiber muscle mechanics were performed (15°C) (Table 1). The *15b-108* hinge-switch flies had a decreased flight performance compared to *15b-47* in terms of flight index, in agreement with previous measurements performed at 25°C (3). The wing-beat frequency of the *15b-108* flies was also decreased compared to the *15b-47* flies at both temperatures. Of interest, reducing the temperature from 22°C

TABLE 1 Flight performance of 15b transgenic flies

	22°C		15°C	
Line	Flight index	WBF (Hz)	Flight index	WBF (Hz)
PwMhc2	4.4 ± 0.2	194 ± 2	4.4 ± 0.3	153 ± 2[‡]
15b-47	1.1 ± 0.5[*,†]	167 ± 4[*,†]	0.9 ± 0.1[*,†]	139 ± 2[*,†,‡]
15b-108	0.2 ± 0.1[*]	142 ± 4[*]	0.4 ± 0.1[*]	121 ± 3[*,‡]

WBF, wing-beat frequency.
*Significant difference ($p < 0.05$) from control (*PwMhc2*).
[†]*15b-47* significantly different ($p < 0.05$) from *15b-108*.
[‡]Significant difference ($p < 0.05$) from 22°C.

TABLE 2 Summary of live, whole fly IFM small angle x-ray diffraction

Line	14.5 Spacing (nm)	14.5 Intensity (%)	Intensity ratio ($I_{2,0}/I_{1,0}$)	Disorder parameter (%)	Interfilament spacing (nm)
PwMhc2	14.42 ± 0.02 (3)	2.96 ± 0.58 (3)	0.95 ± 0.02 (9)	1.31 ± 0.06 (9)	48.4 ± 0.1 (9)
15b-47	14.46 ± 0.02 (5)	2.73 ± 0.51 (5)	0.99 ± 0.02 (9)	1.37 ± 0.05 (9)	49.0 ± 0.2*,† (9)
15b-108	14.41 ± 0.02 (5)	2.87 ± 0.35 (5)	0.98 ± 0.03 (9)	1.43 ± 0.05 (9)	48.5 ± 0.2 (9)

() Number of flies tested.
Temperature, 22–23°C.
*Significant difference ($p < 0.05$) from control (*PwMhc2*).
†*15b-47* significantly different ($p < 0.05$) from *15b-108*.

to 15°C decreased the wing-beat frequency of both the hinge-switch and control lines by 15–21% without a corresponding change in flight index.

Electron microscopy

Bare zone lengths at the center of the A-band were similar for *PwMhc2* (127 ± 3 nm, $n = 41$), *15b-47* (128 ± 3, $n = 41$) and *15b-108* (125 ± 5 nm, $n = 22$). In conjunction with the previously observed increases in A-band length in the hinge-switch compared to control lines (3), this result indicates a longer myosin-containing region in the hinge-switch lines. The ends of the actin filaments were difficult to distinguish, which prevented precise length measurements, but the thin filaments spanned the entire distance from the Z-disk to the M-line in both wild-type and hinge-switch lines, indicating that the increased length of the myosin-containing region in the hinge-switch lines were overlapped entirely by actin filaments.

X-ray diffraction

The in vivo x-ray diffraction patterns of the hinge-switch IFMs were virtually identical to the transgenic control since no changes were observed in the 14.5 spacing and intensity, intensity ratio, or disorder parameter (Table 2). These results indicate that the spacing of the cross-bridges along the thick filaments, cross-bridge orientation with respect to the thick and thin filament, and lattice order are similar between the hinge-switch mutants and the control under resting (wings folded) conditions. The slight increase (1.0–1.2%) in the interfilament spacing of the *15b-47* flies compared to the *15b-108* and *PwMhc2* flies was found to be statistically significant, but it does not appear to affect muscle performance compared to *15b-108*.

Single muscle-fiber mechanics

Relaxed, active, and cross-bridge-dependent isometric tension values were similar between the hinge-switch and *PwMhc2* lines (Table 3). The relationship between isometric tension and calcium concentration showed no significant differences in pCa_{50} values and Hill coefficients (Table 3), suggesting that thin filament regulation does not change with the hinge-switch mutation. At peak calcium activation (pCa 5.0), the magnitudes of elastic modulus, viscous modulus, work output, and power output for hinge-switch fibers were indistinguishable from *PwMhc2* fibers (Fig. 1). Of interest, the oscillatory frequency at which maximum work occurs was significantly higher (22–34%) for the hinge-switch than the *PwMhc2* fibers (Fig. 1 and Table 4), suggesting that the S2/LMM hinge region affects myosin kinetics. However, the oscillatory frequency at which maximum power occurs (*PwMhc2*: 121 ± 4, *15b-47*: 124 ± 3, *15b-108*: 128 ± 3 Hz) was unchanged among the various lines (Fig. 1). The relaxed (pCa 8, where no myosin cross-bridges are strongly attached to actin) and rigor (no ATP, where myosin cross-bridges are strongly attached) conditions showed no changes in elastic or viscous moduli over the entire frequency range examined between hinge-switch and *PwMhc2* fibers (Fig. 2).

To relate sinusoidal analysis with specific steps in the cross-bridge cycle, the complex modulus at peak calcium activation was characterized by the following mathematical expression (37): $Y(\omega) = A(2\pi f\, i/\alpha)^k - B\ if/(b + if) + C\ if/(c + if)$ where A, B, and C are magnitudes expressed in mN/mm^2, b and c are characteristic frequencies expressed in Hz, f = the frequency of the length perturbation (Hz), $i = -1^{1/2}$, $\alpha = 1$ Hz, and k = a unitless exponent. For example, the complex modulus for a *PwMhc2* fiber was fit using the above equation (Fig. 3, *inset*) and broken down into its three processes (A, B, and C). The A-process (described by parameters A and k) is a linear relationship between the viscous and elastic moduli, and the B-process (described by parameters B and b) and C-process (described by parameters C and c) are semicircles (Fig. 3). These six parameters have been related to various aspects of muscle mechanics through experimentation and modeling

TABLE 3 Summary of isometric data from isolated IFM

	Tension (mN/mm^2)				Hill fit parameters		
Line	Active (pCa = 5.0)	Relaxed (pCa = 8.0)	Cross-bridge Dep. (Active–relaxed)	n	pCa_{50}	Hill coefficient	n
PwMhc2	3.2 ± 0.3	2.1 ± 0.2	1.1 ± 0.2	14	5.9 ± 0.1	1.5 ± 0.2	11
15b-47	3.1 ± 0.4	2.0 ± 0.3	1.3 ± 0.3	10	5.9 ± 0.1	1.4 ± 0.2	11
15b-108	2.9 ± 0.3	1.8 ± 0.2	1.1 ± 0.1	11	6.0 ± 0.1	1.5 ± 0.2	12

Isometric tension and Hill fit data from isolated IFM. Cross-bridge Dep., Cross-bridge dependent. Temperature, 15°C.

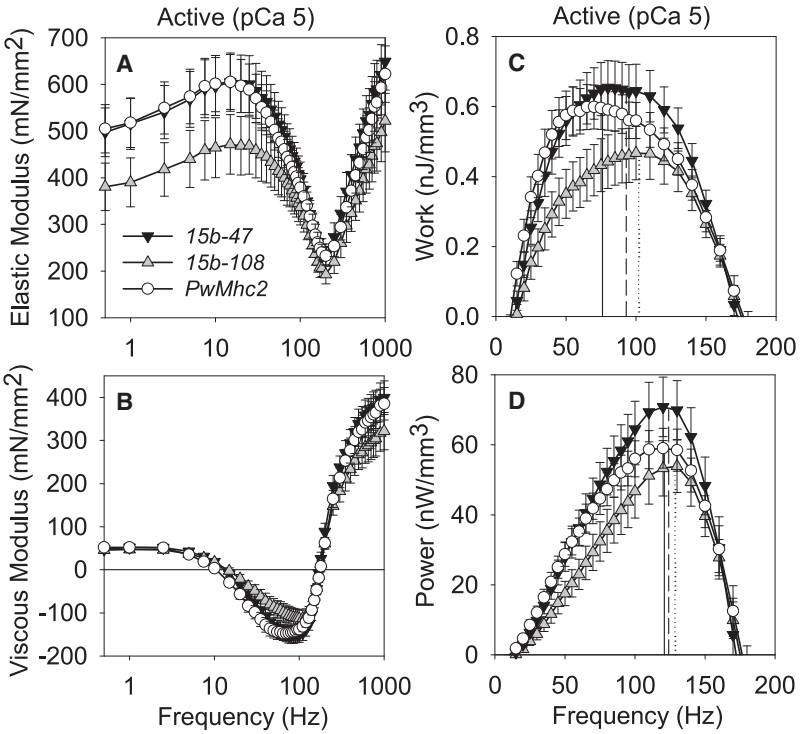

FIGURE 1 Elastic modulus (*A*), viscous modulus (*B*), work (*C*), and power (*D*) for active IFM fibers across muscle oscillation frequencies for hinge-switch (*15b-47* and *15b-108*) and control (*PwMhc2*) lines. Solid (*PwMhc2*), dashed (*15b-47*), and dotted (*15b-108*) lines in *C* and *D* represent frequency of maximum work and power, respectively, from text. Temperature, 15°C.

(44–47). Although different models vary in their precise interpretation, the following summarizes our current thoughts on the meaning of these parameters. For the C-process, $(2\pi c)^{-1}$ represents the average myosin attachment time to actin, t_{on}, and C is equivalent to the number of myosin heads strongly bound to actin multiplied by the cross-bridge stiffness (44). The magnitude part of the B-process (B) is proportional to the number of myosin heads strongly bound to actin and the cross-bridge stiffness (45), and is therefore proportional to C. The frequency portion of the B-process ($2\pi b$) is hypothesized to represent the apparent (observed) rate of myosin force production or, in other words, the rate of myosin transition between the weakly and strongly bound states (46). The A-process reflects the relaxed viscoelastic properties of the structural elements of the fiber, including a portion that increases with Ca^{2+} ascribed to the properties of attached myosin heads (47).

The process magnitudes (A, B and C) remained similar among all three lines, whereas the parameters attributed to myosin kinetics (b and c) and structural properties of the fiber (k) were significantly different between the hinge-switch mutants and *PwMhc2* (Fig. 4). Average myosin attachment time, t_{on}, was calculated using $(2\pi c)^{-1}$ and was increased 15–16% in the hinge-switch mutants compared to *PwMhc2* (*PwMhc2*: 1.22 ± 0.03, *15b-47*: 1.41 ± 0.03, *15b-108*: 1.40 ± 0.06 ms). The 10–22% increase in b suggests that the rate of myosin transition between the weakly and strongly bound states is increased in the hinge-switch mutants. The increase in k indicates an increase in the viscous to elastic modulus ratio in the hinge-switch mutants compared to *PwMhc2*, i.e., that the viscous modulus is greater for a corresponding elastic modulus in the hinge-switch mutants compared to the control.

ATPase and in vitro motility assays

Basal and actin-activated MgATPase rates remained similar when the hinge-switch isoforms were compared with wild-type myosin, which suggests that changing the hinge region does not perturb the maximal ATPase activity in either the presence or absence of actin (Table 5). On the other hand, a reduction in the K_M was observed in the hinge-switch

TABLE 4 Summary of sinusoidal analysis data at maximum work output from isolated IFM

Line	W_{max} (nJ mm^{-3})	f_{Wmax} (Hz)	E_e (mN mm^{-2})	E_v (mN mm^{-2})	Dynamic amplitude (mN mm^{-2})	n
PwMhc2	0.62 ± 0.06	76 ± 5	447 ± 46	−153 ± 16	473 ± 48	15
15b-47	0.68 ± 0.08	93 ± 5*	426 ± 44	−158 ± 18	455 ± 47	15
15b-108	0.49 ± 0.08	102 ± 5*	341 ± 43	−119 ± 21	362 ± 47	13

Averaged sinusoidal analysis data at pCa 5.0. Values are mean ± SE. Maximum work (W_{max}) occurs at specific oscillatory frequencies (f_{Wmax}). E_e refers to the elastic (in-phase) modulus. E_v refers to the minimum viscous (out-of-phase) modulus. Dynamic amplitude is the vector sum of E_e and E_v. Temperature, 15°C.
*Significant difference ($p < 0.05$) from control (*PwMhc2*).

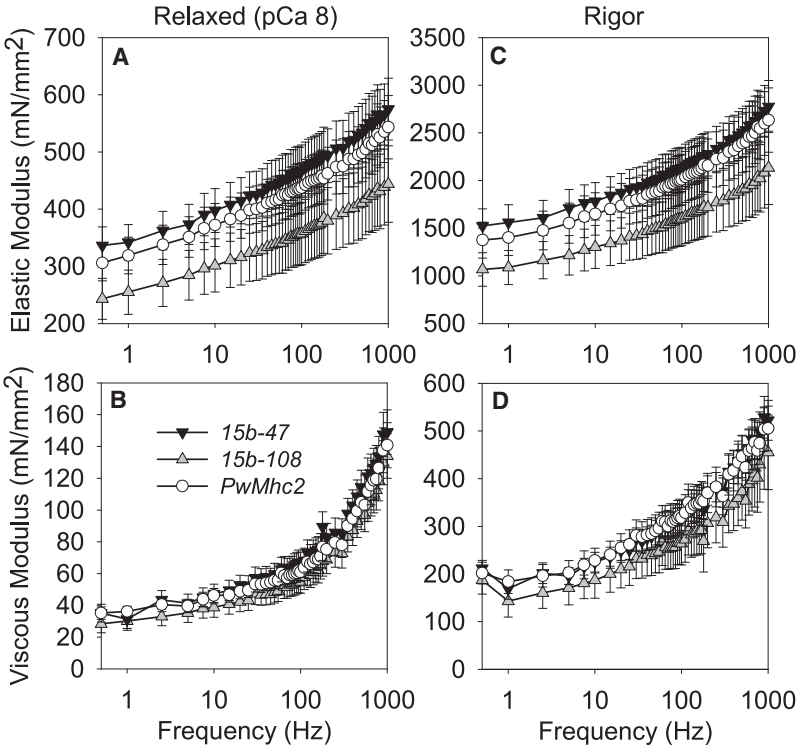

FIGURE 2 Elastic and viscous modulus values for relaxed (*A* and *B*) and rigor (*C* and *D*) IFM fibers across muscle oscillation frequencies for hinge-switch (*15b-47* and *15b-108*) and control (*PwMhc2*) lines. Temperature, 15°C.

myosin compared to wild-type myosin (Table 5), indicating a possible alteration in the affinity of cycling myosin heads for actin. Actin sliding velocities from the in vitro motility assay were similar between the hinge-switch and wild-type myosin (Table 5).

DISCUSSION

We investigated the effects of alternative S2/LMM hinge regions on *D. melanogaster* IFM and found both structural changes and differences in kinetics between myosins containing the endogenous hinge A found in fast contracting muscle and the genetically-inserted hinge B typically found in slow contracting muscle. As discussed below, we hypothesize that the decreased whole-fly muscle performance in the hinge-switch lines is due to sarcomere length increases as well as kinetic changes at the level of the acto-myosin cross-bridge.

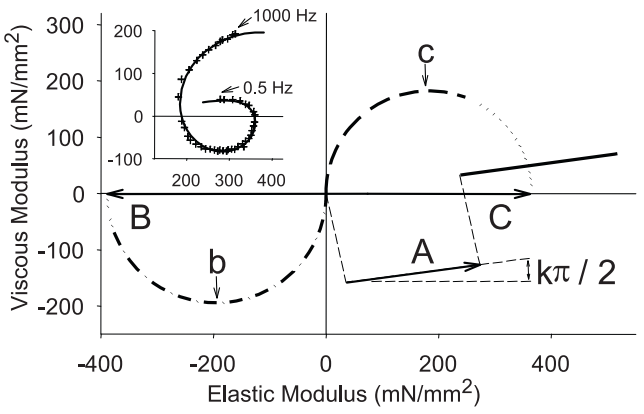

FIGURE 3 (*Inset*) Complex modulus recorded at frequencies ranging from 0.5 to 1000 Hz (+) for a control (*PwMhc2*) fiber at pCa 5 and 15°C is well-characterized by the solid line calculated using the equation in the text. The complex modulus, shown in the inset, can be attributed to three underlying processes (processes A–C). The A-process (described by parameters *A* and *k*) is a linear relationship, and the B-process (described by parameters *B* and *b*) and C-process (described by parameters *C* and *c*) are semicircles.

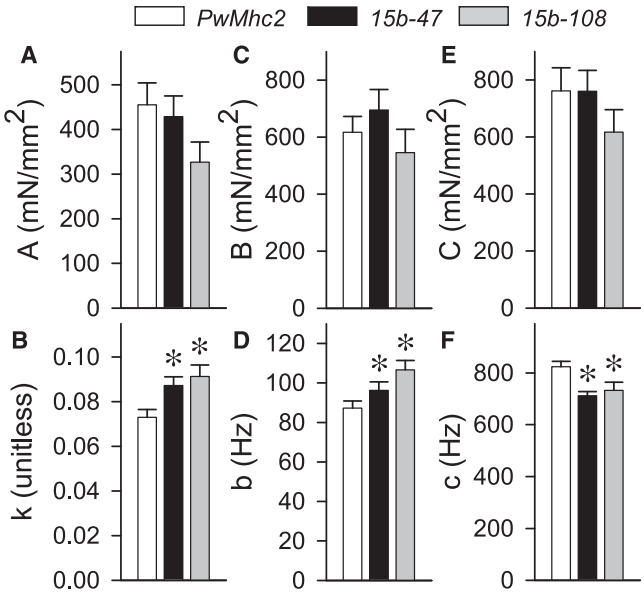

FIGURE 4 A- (panels *A* and *B*), B- (panels *C* and *D*), and C- (panels *E* and *F*) process parameters from active IFM fibers for hinge-switch (*15b-47* and *15b-108*) and control (*PwMhc2*) lines. * Significant difference ($p < 0.05$) from the control line.

TABLE 5 Steady-state kinetic parameters and actin-sliding velocities for wild-type and *15b* myosins

Myosin isoform	Basal MgATPase (s^{-1} $head^{-1}$)	Actin-activated V_{max} (s^{-1} $head^{-1}$)	K_M actin (μM)	n	Actin sliding velocity ($\mu m\ s^{-1}$)	n
Wild-type	0.22 ± 0.01	1.70 ± 0.13	0.31 ± 0.05	11	7.4 ± 0.1	3
15b	0.17 ± 0.01	1.57 ± 0.12	0.12 ± 0.04*	5	7.5 ± 0.1	3

Temperature, 22–23°C.
*Significant difference ($p < 0.05$) from wild-type.

These findings highlight the importance of the S2/LMM hinge region in regulating sarcomere structure as well as myosin kinetics and, in turn, muscle functional performance. Of importance, this is the first study, to our knowledge, that examines the effects of the S2/LMM hinge region on active single-fiber mechanics and actin-myosin kinetics when only this specific region of the myosin molecule is different.

Muscle structure

A profound structural change previously observed in the electron micrographs of myofibrils from the hinge-switch lines was an increase in sarcomere length, primarily due to an increase in the A-band length, as compared to the control line (3). Sarcomere length and A-band length increases were similar between 2-day-old mature flies (13%) and those <2 h old (6–12%), indicating that these increases were present at or near the time of eclosion (3). Similar increases in sarcomere length (6–9%) were found using light microscopy in resting hinge-switch myofibrils from 2-day-old mature adult flies compared to the transgenic control (48), indicating that the morphological changes were not due to fixation artifacts.

In this study, we sought to determine the reason for the increase in A-band length in the hinge-switch lines. The in vivo 14.5 nm myosin head spacing, measured using x-ray diffraction, and the length of the A-band bare zone, determined using electron microscopy, remained similar between the hinge-switch lines and their transgenic control. These results indicate that the increased A-band length in fibers containing hinge B is due to an increase in the number of myosin molecules incorporated longitudinally in the thick filament. An increase in the number of myosin heads along the thick filament could have significant effects on single-fiber performance, especially since a corresponding increase in actin filament length apparently occurs, resulting in a longer myosin-actin overlap region in the hinge-switch lines. Our current results strengthen the notion, proposed in a previous study (3), that the S2/LMM hinge region plays an important regulatory role in determining in vivo thick and thin filament lengths as well as sarcomere length. We postulate that hinge B increases thick filament length by enhancing the rate of myosin polymerization into thick filaments during sarcomere assembly. The enhanced rate is most likely due to an increased ability of hinge B to interact with other myosin molecules and/or thick filament proteins, a possible outcome if the coiled-coil of hinge B has a more stable configuration than that of hinge A (3). We also postulate that the increase in thin filament length in the hinge B lines occurs during development in response to the longer thick filaments. This hypothesis is supported by evidence that sarcomere length and thick and thin filament length elongate by the same amount during development, indicating that thick and thin filament lengths are highly regulated and probably extend in relation to one another (49). Additionally, removal of flightin, a thick-filament-associated protein, uniformly increases thick and thin filament length (~20%) in late-stage pupa (50), indicating that increases in thick filament length can drive similar elongation of the thin filament.

The in vivo myosin head spacing (~14.5 nm) is similar between the lines despite the previous finding that individually isolated myosin molecules from the hinge-switch lines had longer tail regions (~5 nm) than their transgenic control (3). This observed increase in rod length agreed with software predictions that hinge B in the hinge-switch lines would be more likely to form a coiled-coil than the hinge A in the control line (3), since a coiled-coil structure is calculated to be longer than a random helix (11). This increased myosin tail length must either be 1), incorporated into the thick filament backbone, leaving the free S2 length similar between the hinge-switch and controls; or 2), unincorporated into the thick filament backbone, increasing the S2 length free of the thick filament backbone in the hinge-switch lines compared to control. Recent experiments in the giant water bug *Lethocerus* suggest that only ~10 nm of the S2 portion flanking the S1/S2 hinge is free of the thick filament backbone (51). This result suggests that the S2/LMM hinge region is incorporated into the thick filament since the hinge region lies between 44 and 76 nm from the S1/S2 hinge (8). However, *Drosophila* and *Lethocerus* contain different IFM proteins and protein levels (52–54) that could lead to differences in myosin incorporation into the thick filament. A definitive resolution of how the S2/LMM hinge incorporates into the thick filament backbone awaits future structural studies in *Drosophila* of the kind performed in *Lethocerus*.

In vivo interfilament spacings remain the same or slightly higher in the hinge-switch lines when directly measured in relaxed live *Drosophila* fibers (wings down) using x-ray diffraction. Previous ultrastructure studies showed that the myofibril CSA decreased in 2-day-old mature hinge-switch adult flies compared to controls in both skinned myofibrils (48) and fixed and embedded myofibrils (3), yet the number of thick filaments per myofibril remained unchanged (3).

These previous results imply that the myofibril interfilament spacing (center-to-center distance between thick filaments) decreased in the hinge-switch lines, contrary to the x-ray diffraction results presented here. To explain the previously found decrease in myofibrillar CSA of the hinge-switch lines, we postulate that a reduction in transverse stiffness occurs in these lines due to the decreased number of Z-bands per unit length that accompany the increased sarcomere lengths (55,56). A decreased transverse stiffness would make the hinge-switch lines more susceptible to the compression known to occur during fixation and embedding for electron microscopy (57). In addition, the decreased transverse stiffness would reduce the outward force exerted by the Z-bands to maintain lattice structure, causing the hinge-switch myofibrils to expand less than controls when skinned.

The x-ray diffraction data showing that the hinge-switch lines' 14.5 nm intensity and intensity ratios are comparable to the transgenic control indicate that cross-bridge orientation, with respect to the thick and thin filament, remains similar regardless of the S2/LMM hinge. Lattice disorder is also similar between the various lines tested, indicating that the change in hinge region does not introduce any significant changes to this parameter, despite the occasional minor defects (e.g., disrupted M-lines and rough edges) previously observed in electron micrographs (3). Since myosin orientation, myosin head spacing, interfilament spacing, and lattice order remain unchanged between the hinge-switch lines and the transgenic control, the primary structural differences within the myofilament lattice are the increased sarcomere and A-band lengths.

Single-fiber mechanics and actin-myosin kinetics

Although the S2/LMM hinge region is distant from the myosin head, a switch in isoform alters myosin kinetics. Single-fiber experiments indicate that hinge B, found in the hinge-switch mutants, increases the time myosin spends in the strongly bound state, as evidenced by the increase in myosin attachment time (15–16%) compared to hinge A in the control line. Single-fiber experiments also show increases in the oscillatory frequency at which maximum work occurs (22–34%) and the rate of myosin transition between the weakly and strongly bound states (10–22%). Steady-state kinetics indicates that hinge B increases the affinity of myosin for actin, as shown by the decrease in K_M (61%). The increase in affinity of myosin for actin differed substantially in myosins with hinge B versus hinge A for the full-length samples (initial slopes in Fig. 5). The marked difference between hinge B and A was not evident for S1 alone (data not shown), indicating that the increased affinity of myosin for actin requires the presence of the hinge-containing rod. The lack of changes in actin-activated V_{max}, which is rate-limited by ATP hydrolysis (58), suggests that the hinge region does not appreciably change the duration of the detached states. A change in myosin step size does not appear to account for the altered myosin kinetics, since we previously found no difference in step size between myosins containing hinge A (IFM isoform) and those containing hinge B (embryonic isoform) (41).

How can a change in the S2/LMM hinge region affect myosin kinetics, especially given the distance of this hinge region from the myosin head? We speculate that the increase in tail length of myosins containing hinge B, compared to myosins containing hinge A (3), permits the myosin head to more easily find an actin-binding site and to remain attached to actin longer. This would explain our observed increases in actin affinity and longer myosin attachment time in the hinge-switch lines compared to control. Notably, our hypothesis suggests that the hinge region remains free of the thick filament backbone so that the increase in length will affect the myosin head kinetics.

Other structural and mechanical differences due to changes in the S2/LMM hinge region could alter myosin kinetics. First, hinge B is more likely to form a coiled-coil than hinge A, based on structure-prediction software, and may be why hinge B myosin molecules have a longer tail (3). In vitro experiments and molecular simulations suggest that a coiled-coil is stiffer than a random helix in the longitudinal (10), lateral (59,60), and rotational directions (11). However, recent modeling results indicate that an increase in cross-bridge stiffness should increase the cross-bridge detachment rate (61), which should decrease myosin attachment time, opposite to our hinge-switch single-fiber results. Second, incorporating hinge A or B into the myofilament lattice may affect myosin molecule packing and between-filament interactions due to differences in hydrophobicity and charge distribution between the hinges (3). For instance, an interaction between the S2/LMM hinge region of one myosin molecule and the myosin head of an adjacent

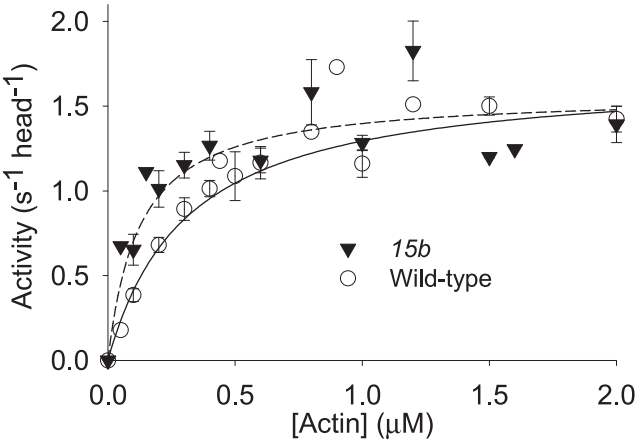

FIGURE 5 Actin-activated Mg^{2+}-ATPase activity of hinge-switch (*15b*) and control (wild-type) myosin. The maximal ATPase activity does not differ between the two myosins, but an increase in the affinity of cycling myosin heads for actin (K_M) is found for the hinge-switch myosin.

molecule has been proposed to explain differences in smooth muscle performance after addition of an antibody to the hinge region (62). However, we observe differences in the kinetics of isolated myosin where packing and between-filament interactions are absent. Lastly, changes in the S2/LMM hinge region may affect the ability of this region to melt, or transform from a coiled-coil to a random helix (5,12,13).

The hinge-switch lines produced no significant differences in active or rigor tension, oscillatory work or power, or the model-based parameters B and C. These measures depend on the number of cross-bridges bound and the cross-bridge stiffness, indicating that the relatively subtle changes in myosin kinetics, such as the 15–16% increase in myosin attachment time, did not significantly affect these parameters between the hinge-switch and control lines. This is not surprising considering that large changes ($\geq$50%) in myosin kinetics are typically required to produce differences in active tension (63–65), most likely due to the low active to relaxed tension ratio in *Drosophila* IFM fibers.

Although the hinge-switch lines showed a number of differences in myosin kinetics, it should be noted that the actin sliding velocity from in vitro motility measurements, an indicator of myosin attachment time, binding kinetics, and step size (66), was unchanged. However, our in vitro motility techniques produce nonspecific binding of the myosin molecule to the coverslip, which may result in the myosin molecule binding between the end of the myosin head and the start of the S2/LMM hinge region. In this case, the changes in S2/LMM hinge length would not affect cross-bridge kinetics, making myosin containing hinge B perform similarly to myosin with hinge A. Previous research has shown that the portion of myosin attached to the surface influences its flexibility and in vitro motility (67).

The S2/LMM hinge does not affect the relaxed mechanical properties of muscle fibers with respect to isometric tension, as well as elastic and viscous moduli, in agreement with previous work in myofibrils and single muscle fibers (48). The relaxed properties of single IFM fibers are expected to arise from the extension of C-filaments, composed of kettin (68) and/or projectin (69), that connect the thick filaments to the Z-disk (70). The C-filaments provide the majority of the IFM fiber's extensibility due to their being less stiff, or more easily stretched, than the comparatively stiff thick filaments. The increase in sarcomere length in the hinge-switch lines occurs in parallel with an increase in thick filament length, leaving the distance between the ends of the thick filament and the Z-disk similar to the control line. Hence, the C-filaments of the hinge-switch and control lines are similarly stretched, yielding similar relaxed mechanical properties. The lack of differences between the hinge-switch and control lines in fibers (relaxed properties determined by small amplitude oscillations) and myofibrils (relaxed properties determined by elongation) (48) suggest that hinge B does not drastically alter thick filament stiffness or the strain response of the C-filaments.

Flight performance

The large decrease in flight index (75–95%) for the hinge-switch lines compared to the control line is most likely driven by the reduction in wing-beat frequency (9–27%). We hypothesize that the reduced wing-beat frequency in the hinge-switch lines is caused by their increased sarcomere length and increased myosin attachment time, as *Drosophila*'s wing-beat frequency is partially influenced by the contraction velocity of its muscle fibers. On the fiber level, the velocity of muscle fiber contraction is equal to the total number of sarcomeres in the muscle fiber multiplied by sarcomere contraction velocity. IFM fibers from the hinge-switch and control lines were found to have similar fiber lengths within the thorax when observed during dissections. Thus, since the hinge-switch lines have 13% longer sarcomeres than controls but the same fiber length, the hinge-switch lines would have 13% fewer total sarcomeres than the control, resulting in a 13% decrease in contraction velocity using the equation above. At the sarcomere level, the increase in myosin attachment time (15–16%) should decrease the sarcomere contraction velocity due to the increased drag of a myosin head attached for a longer period of time. Thus, the sarcomere length and myosin kinetic differences of the hinge-switch lines most likely drive *Drosophila*'s decreased wing-beat frequency and flight performance as compared to the control.

Relevance to vertebrate MHCs

Comparisons of the amino acid sequences of the eight human MHCs, two cardiac (α and β) MHCs, and six skeletal MHCs (IIa, IIb, IIx/d, embryonic, perinatal, and extraocular) show that their full-length identity ranges from 77% to 95% (18). Notably, head and rod sequence comparisons within each MHC isoform reveal that the percent identity of amino acid sequences of most heads is similar to that of their rods (18). This high percent identity suggests that the rod portion of the MHC plays an important role in determining the functional and structural properties of the myosin, perhaps on the same order as the head. Our results in *Drosophila* indicate that one role of the MHC rod, specifically the S2/LMM region, is to provide a small influence on myosin and muscle kinetics. This may also be the case in vertebrates. For example, replacing portions of the nonidentical α-MHC head sequences with β-MHC head sequences in mice produced myosins that performed similarly to β-MHC in some aspects, but not completely (71,72), leaving open the possibility that the S2/LMM region may affect cardiac myosin kinetics in vertebrates. Our findings also suggest that another role of the S2/LMM hinge region in *Drosophila* is to regulate in vivo thick and thin filament lengths as well as sarcomere length, which may be the case in vertebrates as well. The functional and structural changes that result from switching the S2/LMM hinge regions in *Drosophila* IFM suggest that examining the role of this region within

vertebrate muscle may provide important insights into myosin isoform-specific properties.

CONCLUSIONS

Replacement of the S2/LMM fast muscle isovariant hinge A with the slow muscle hinge B in the IFMs of *Drosophila* caused decreases in flight performance, which can be explained by the concurrent increases in sarcomere length and myosin attachment time. The longer sarcomere lengths in the hinge-switch lines appear to be caused by the longitudinal addition of myosin heads since their myosin head spacing (14.5 nm spacing) and A-band bare zone length were similar to the transgenic control. The increased actin affinity, myosin attachment time, and rate of myosin transition between the weakly and strongly bound states found in the hinge-switch lines suggest that the increased length of the S2/LMM hinge region affects myosin performance. These results indicate that the S2/LMM hinge region, despite its distance from the myosin head, affects myosin kinetics and has an important regulatory role in determining in vivo thick and thin filament lengths as well as sarcomere length in the *Drosophila* IFM.

We thank Jennifer A. Suggs for electron microscopy work, Anju Melkani for help with several myosin preparations, and Dr. Girish C. Melkani for performing a portion of the ATPase assays.

This work was supported by grants from the National Institutes of Health (NIH; R01 AR049425 to D.W.M., R01 AR043396 to S.I.B., and R01 AR055611 to D.M.S.). Advanced Photon Source use was supported by the U.S. Department of Energy, Basic Energy Sciences, Office of Science under contract No. W-31-109-ENG-38. BioCAT is an NIH-supported research center (RR-08630). The content is solely the responsibility of the authors and does not necessarily reflect the official views of the National Center for Research Resources or the NIH.

REFERENCES

1. Stewart, M., and P. Edwards. 1984. Length of myosin rod and its proteolytic fragments determined by electron microscopy. *FEBS Lett.* 168:75–78.
2. Stewart, M., and G. C. K. Roberts. 1982. H NMR study of long and short myosin S2 fragments. *FEBS Lett.* 146:293–296.
3. Suggs, J. A., A. Cammarato, W. A. Kronert, M. Nikkhoy, C. M. Dambacher, et al. 2007. Alternative S2 hinge regions of the myosin rod differentially affect muscle function, myofibril dimensions and myosin tail length. *J. Mol. Biol.* 367:1312–1329.
4. Huxley, H. E. 1969. The mechanism of muscular contraction. *Science.* 164:1356–1365.
5. Burke, M., S. Himmelfarb, and W. F. Harrington. 1973. Studies on the ''hinge'' region of myosin. *Biochemistry.* 12:701–710.
6. Lowey, S., H. S. Slayter, A. G. Weeds, and H. Baker. 1969. Substructure of the myosin molecule. I. Subfragments of myosin by enzymic degradation. *J. Mol. Biol.* 42:1–29.
7. McLachlan, A. D., and J. Karn. 1982. Periodic charge distributions in the myosin rod amino acid sequence match cross-bridge spacings in muscle. *Nature.* 299:226–231.
8. Walker, M., P. Knight, and J. Trinick. 1985. Negative staining of myosin molecules. *J. Mol. Biol.* 184:535–542.
9. Lu, R. C., and A. Wong. 1985. The amino acid sequence and stability predictions of the hinge region in myosin subfragment 2. *J. Biol. Chem.* 260:3456–3461.
10. Root, D. D., V. K. Yadavalli, J. G. Forbes, and K. Wang. 2006. Coiled-coil nanomechanics and uncoiling and unfolding of the superhelix and α-helices of myosin. *Biophys. J.* 90:2852–2866.
11. Gundapaneni, D., J. Xu, and D. D. Root. 2005. High flexibility of the actomyosin crossbridge resides in skeletal muscle myosin subfragment-2 as demonstrated by a new single molecule assay. *J. Struct. Biol.* 149:117–126.
12. Tsong, T. Y., S. Himmelfarb, and W. F. Harrington. 1983. Stability and melting kinetics of structural domains in the myosin rod. *J. Mol. Biol.* 164:431–450.
13. Walzthony, D., H. M. Eppenberger, H. Ueno, W. F. Harrington, and T. Wallimann. 1986. Melting of myosin rod as revealed by electron microscopy. II. Effects of temperature and pH on length and stability of myosin rod and its fragments. *Eur. J. Cell Biol.* 41:38–43.
14. Nyitray, L., A. Jancso, Y. Ochiai, L. Graf, and A. G. Szent-Gyorgyi. 1994. Scallop striated and smooth muscle myosin heavy-chain isoforms are produced by alternative RNA splicing from a single gene. *Proc. Natl. Acad. Sci. USA.* 91:12686–12690.
15. Collier, V. L., W. A. Kronert, P. T. O'Donnell, K. A. Edwards, and S. I. Bernstein. 1990. Alternative myosin hinge regions are utilized in a tissue-specific fashion that correlates with muscle contraction speed. *Genes Dev.* 4:885–895.
16. Hastings, G. A., and C. P. Emerson, Jr. 1991. Myosin functional domains encoded by alternative exons are expressed in specific thoracic muscles of *Drosophila*. *J. Cell Biol.* 114:263–276.
17. McNally, E. M., R. Kraft, M. Bravo-Zehnder, D. A. Taylor, and L. A. Leinwand. 1989. Full-length rat α and β cardiac myosin heavy chain sequences. Comparisons suggest a molecular basis for functional differences. *J. Mol. Biol.* 210:665–671.
18. Weiss, A., S. Schiaffino, and L. A. Leinwand. 1999. Comparative sequence analysis of the complete human sarcomeric myosin heavy chain family: implications for functional diversity. *J. Mol. Biol.* 290:61–75.
19. Lovell, S., T. Karr, and W. F. Harrington. 1988. Suppression of contractile force in muscle fibers by antibody to myosin subfragment 2. *Proc. Natl. Acad. Sci. USA.* 85:1849–1853.
20. Harrington, W. F., T. Karr, W. B. Busa, and S. J. Lovell. 1990. Contraction of myofibrils in the presence of antibodies to myosin subfragment 2. *Proc. Natl. Acad. Sci. USA.* 87:7453–7456.
21. Sugi, H., T. Kobayashi, T. Gross, K. Noguchi, T. Karr, et al. 1992. Contraction characteristics and ATPase activity of skeletal muscle fibers in the presence of antibody to myosin subfragment 2. *Proc. Natl. Acad. Sci. USA.* 89:6134–6137.
22. Margossian, S. S., J. W. Krueger, J. R. Sellers, G. Cuda, J. B. Caulfield, et al. 1991. Influence of the cardiac myosin hinge region on contractile activity. *Proc. Natl. Acad. Sci. USA.* 88:4941–4945.
23. Liu, H., M. S. Miller, D. M. Swank, W. A. Kronert, D. W. Maughan, et al. 2005. Paramyosin phosphorylation site disruption affects indirect flight muscle stiffness and power generation in *Drosophila melanogaster*. *Proc. Natl. Acad. Sci. USA.* 102:10522–10527.
24. Miller, B. M., M. Nyitrai, S. I. Bernstein, and M. A. Geeves. 2003. Kinetic analysis of *Drosophila* muscle myosin isoforms suggests a novel mode of mechanochemical coupling. *J. Biol. Chem.* 278:50293–50300.
25. George, E. L., M. B. Ober, and C. P. Emerson, Jr. 1989. Functional domains of the *Drosophila melanogaster* muscle myosin heavy-chain gene are encoded by alternatively spliced exons. *Mol. Cell. Biol.* 9:2957–2974.
26. Swank, D. M., L. Wells, W. A. Kronert, G. E. Morrill, and S. I. Bernstein. 2000. Determining structure/function relationships for sarcomeric myosin heavy chain by genetic and transgenic manipulation of *Drosophila*. *Microsc. Res. Tech.* 50:430–442.
27. Drummond, D. R., E. S. Hennessey, and J. C. Sparrow. 1991. Characterisation of missense mutations in the *Act88F* gene of *Drosophila melanogaster*. *Mol. Gen. Genet.* 226:70–80.

28. Tohtong, R., H. Yamashita, M. Graham, J. Haeberle, A. Simcox, et al. 1995. Impairment of muscle function caused by mutations of phosphorylation sites in myosin regulatory light chain. *Nature*. 374:650–653.
29. Hyatt, C. J., and D. W. Maughan. 1994. Fourier analysis of wing beat signals: assessing the effects of genetic alterations of flight muscle structure in Diptera. *Biophys. J.* 67:1149–1154.
30. Irving, T. C., and D. W. Maughan. 2000. *In vivo* x-ray diffraction of indirect flight muscle from *Drosophila melanogaster*. *Biophys. J.* 78:2511–2515.
31. Irving, T. C., R. Fischetti, G. Rosenbaum, and G. B. Bunker. 2000. Fiber diffraction using the BioCAT undulator beamline at the Advanced Photon Source. *Nucl. Instrum. Methods Phys. Res. A.* 448:250–254.
32. Irving, T. C., and B. M. Millman. 1989. Changes in thick filament structure during compression of the filament lattice in relaxed frog sartorius muscle. *J. Muscle Res. Cell Motil.* 10:385–394.
33. Irving, T. C. 2006. X-ray diffraction of indirect flight muscle from *Drosophila* in vivo. *In* Nature's Versatile Engine: Insect Flight Muscle Inside and Out. J. O. Vigoreaux, editor. Landes Bioscience, Georgetown, TX. 197–213.
34. Irving, T., S. Bhattacharya, I. Tesic, J. Moore, G. Farman, et al. 2001. Changes in myofibrillar structure and function produced by N-terminal deletion of the regulatory light chain in *Drosophila*. *J. Muscle Res. Cell Motil.* 22:675–683.
35. Yu, L. C., A. C. Steven, G. R. Naylor, R. C. Gamble, and R. J. Podolsky. 1985. Distribution of mass in relaxed frog skeletal muscle and its redistribution upon activation. *Biophys. J.* 47:311–321.
36. Godt, R. E., and B. D. Lindley. 1982. Influence of temperature upon contractile activation and isometric force production in mechanically skinned muscle fibers of the frog. *J. Gen. Physiol.* 80:279–297.
37. Dickinson, M. H., C. J. Hyatt, F. O. Lehmann, J. R. Moore, M. C. Reedy, et al. 1997. Phosphorylation-dependent power output of transgenic flies: an integrated study. *Biophys. J.* 73:3122–3134.
38. Kawai, M., and P. W. Brandt. 1980. Sinusoidal analysis: a high resolution method for correlating biochemical reactions with physiological processes in activated skeletal muscles of rabbit, frog and crayfish. *J. Muscle Res. Cell Motil.* 1:279–303.
39. Kronert, W. A., C. M. Dambacher, A. F. Knowles, D. M. Swank, and S. I. Bernstein. 2008. Alternative relay domains of *Drosophila melanogaster* myosin differentially affect ATPase activity, *in vitro* motility, myofibril structure and muscle function. *J. Mol. Biol.* 379:443–456.
40. Pardee, J. D., and J. A. Spudich. 1982. Purification of muscle actin. *Methods Enzymol.* 85:164–181, (Pt. B).
41. Swank, D. M., M. L. Bartoo, A. F. Knowles, C. Iliffe, S. I. Bernstein, et al. 2001. Alternative exon-encoded regions of *Drosophila* myosin heavy chain modulate ATPase rates and actin sliding velocity. *J. Biol. Chem.* 276:15117–15124.
42. Cammarato, A., C. M. Dambacher, A. F. Knowles, W. A. Kronert, R. Bodmer, et al. 2008. Myosin transducer mutations differentially affect motor function, myofibril structure, and the performance of skeletal and cardiac muscles. *Mol. Biol. Cell.* 19:553–562.
43. Root, D. D., and K. Wang. 1994. Calmodulin-sensitive interaction of human nebulin fragments with actin and myosin. *Biochemistry.* 33:12581–12591.
44. Palmer, B. M., T. Suzuki, Y. Wang, W. D. Barnes, M. S. Miller, et al. 2007. Two-state model of acto-myosin attachment-detachment predicts C-process of sinusoidal analysis. *Biophys. J.* 93:760–769.
45. Kawai, M., Y. Saeki, and Y. Zhao. 1993. Crossbridge scheme and the kinetic constants of elementary steps deduced from chemically skinned papillary and trabecular muscles of the ferret. *Circ. Res.* 73:35–50.
46. Zhao, Y., and M. Kawai. 1993. The effect of the lattice spacing change on cross-bridge kinetics in chemically skinned rabbit psoas muscle fibers. II. Elementary steps affected by the spacing change. *Biophys. J.* 64:197–210.
47. Mulieri, L. A., W. Barnes, B. J. Leavitt, F. P. Ittleman, M. M. LeWinter, et al. 2002. Alterations of myocardial dynamic stiffness implicating abnormal crossbridge function in human mitral regurgitation heart failure. *Circ. Res.* 90:66–72.
48. Hao, Y., M. S. Miller, D. M. Swank, H. Liu, S. I. Bernstein, et al. 2006. Passive stiffness in *Drosophila* indirect flight muscle reduced by disrupting paramyosin phosphorylation, but not by embryonic myosin S2 hinge substitution. *Biophys. J.* 91:4500–4506.
49. Reedy, M. C., and C. Beall. 1993. Ultrastructure of developing flight muscle in *Drosophila*. I. Assembly of myofibrils. *Dev. Biol.* 160:443–465.
50. Reedy, M. C., B. Bullard, and J. O. Vigoreaux. 2000. Flightin is essential for thick filament assembly and sarcomere stability in *Drosophila* flight muscles. *J. Cell Biol.* 151:1483–1500.
51. Liu, J., S. Wu, M. C. Reedy, H. Winkler, C. Lucaveche, et al. 2006. Electron tomography of swollen rigor fibers of insect flight muscle reveals a short and variably angled S2 domain. *J. Mol. Biol.* 362:844–860.
52. Maroto, M., J. Arredondo, D. Goulding, R. Marco, B. Bullard, et al. 1996. *Drosophila* paramyosin/miniparamyosin gene products show a large diversity in quantity, localization, and isoform pattern: a possible role in muscle maturation and function. *J. Cell Biol.* 134:81–92.
53. Peckham, M., J. E. Molloy, J. C. Sparrow, and D. C. White. 1990. Physiological properties of the dorsal longitudinal flight muscle and the tergal depressor of the trochanter muscle of *Drosophila melanogaster*. *J. Muscle Res. Cell Motil.* 11:203–215.
54. Qiu, F., S. Brendel, P. M. Cunha, N. Astola, B. Song, et al. 2005. Myofilin, a protein in the thick filaments of insect muscle. *J. Cell Sci.* 118:1527–1536.
55. Yoshikawa, Y., T. Yasuike, A. Yagi, and T. Yamada. 1999. Transverse elasticity of myofibrils of rabbit skeletal muscle studied by atomic force microscopy. *Biochem. Biophys. Res. Commun.* 256:13–19.
56. Akiyama, N., Y. Ohnuki, Y. Kunioka, Y. Saeki, and T. Yamada. 2006. Transverse stiffness of myofibrils of skeletal and cardiac muscles studied by atomic force microscopy. *J. Physiol. Sci.* 56:145–151.
57. Reedy, M. K., R. S. Goody, W. Hofmann, and G. Rosenbaum. 1983. Co-ordinated electron microscopy and X-ray studies of glycerinated insect flight muscle. I. X-ray diffraction monitoring during preparation for electron microscopy of muscle fibres fixed in rigor, in ATP and in AMPPNP. *J. Muscle Res. Cell Motil.* 4:25–53.
58. White, H. D., B. Belknap, and M. R. Webb. 1997. Kinetics of nucleoside triphosphate cleavage and phosphate release steps by associated rabbit skeletal actomyosin, measured using a novel fluorescent probe for phosphate. *Biochemistry.* 36:11828–11836.
59. Adamovic, I., S. M. Mijailovich, and M. Karplus. 2008. The elastic properties of the structurally characterized myosin II S2 subdomain: a molecular dynamics and normal mode analysis. *Biophys. J.* 94:3779–3789.
60. Wolgemuth, C. W., and S. X. Sun. 2006. Elasticity of α-helical coiled coils. *Phys. Rev. Lett.* 97:248101.
61. Tanner, B. C., T. L. Daniel, and M. Regnier. 2007. Sarcomere lattice geometry influences cooperative myosin binding in muscle. *PLoS Comput. Biol.* 3:e115.
62. Cai, S., D. G. Ferguson, A. F. Martin, and R. J. Paul. 1995. Smooth muscle contractility is modulated by myosin tail-S2-LMM hinge region interaction. *Am. J. Physiol.* 269:C1126–C1132.
63. Swank, D. M., J. Braddock, W. Brown, H. Lesage, S. I. Bernstein, et al. 2006. An alternative domain near the ATP binding pocket of *Drosophila* myosin affects muscle fiber kinetics. *Biophys. J.* 90:2427–2435.
64. Swank, D. M., A. F. Knowles, J. A. Suggs, F. Sarsoza, A. Lee, et al. 2002. The myosin converter domain modulates muscle performance. *Nat. Cell Biol.* 4:312–316.
65. Swank, D. M., W. A. Kronert, S. I. Bernstein, and D. W. Maughan. 2004. Alternative N-terminal regions of *Drosophila* myosin heavy chain tune muscle kinetics for optimal power output. *Biophys. J.* 87:1805–1814.
66. Hooft, A. M., E. J. Maki, K. K. Cox, and J. E. Baker. 2007. An accelerated state of myosin-based actin motility. *Biochemistry.* 46:3513–3520.

67. Winkelmann, D. A., L. Bourdieu, A. Ott, F. Kinose, and A. Libchaber. 1995. Flexibility of myosin attachment to surfaces influences F-actin motion. *Biophys. J.* 68:2444–2453.

68. Kulke, M., C. Neagoe, B. Kolmerer, A. Minajeva, H. Hinssen, et al. 2001. Kettin, a major source of myofibrillar stiffness in *Drosophila* indirect flight muscle. *J. Cell Biol.* 154:1045–1057.

69. Saide, J. D., S. Chin-Bow, J. Hogan-Sheldon, L. Busquets-Turner, J. O. Vigoreaux, et al. 1989. Characterization of components of Z-bands in the fibrillar flight muscle of *Drosophila melanogaster*. *J. Cell Biol.* 109:2157–2167.

70. White, D. C. 1983. The elasticity of relaxed insect fibrillar flight muscle. *J. Physiol.* 343:31–57.

71. Krenz, M., A. Sanbe, F. Bouyer-Dalloz, J. Gulick, R. Klevitsky, et al. 2003. Analysis of myosin heavy chain functionality in the heart. *J. Biol. Chem.* 278:17466–17474.

72. Krenz, M., S. Sadayappan, H. E. Osinska, J. A. Henry, S. Beck, et al. 2007. Distribution and structure-function relationship of myosin heavy chain isoforms in the adult mouse heart. *J. Biol. Chem.* 282:24057–24064.